Mechanics of Materials 176 (2023) 104526

Contents lists available at ScienceDirect

Mechanics of Materials

journal homepage: www.elsevier.com/locate/mechmat

# Development of a new approach for corrosion-fatigue analysis of offshore steel structures

Helen Ryan [a], Ali Mehmanparast [b,*]

[a] Offshore Renewable Energy Engineering Centre, Cranfield University, Cranfield, MK43 0AL, UK
[b] Department of Naval Architecture, Ocean and Marine Engineering, University of Strathclyde, Glasgow G1 1XQ, UK

ARTICLE INFO

*Keywords:*
Corrosion-fatigue model
Corrosion-fatigue parameter
Frequency
Seawater
Offshore structures

ABSTRACT

Corrosion-fatigue is known to be the dominant failure mechanism in offshore structures, such as offshore wind turbines, due to the constant exertion of cyclic loads in highly corrosive environments. In the present study, the existing corrosion-fatigue crack growth (CFCG) theories and models have been firstly reviewed and discussed, and subsequently a new approach has been proposed to accurately describe the corrosion-fatigue behaviour under various loading conditions and frequencies. To examine the validity of the proposed approach, fatigue crack growth experiments were conducted on S355G10+M medium strength steel compact tension, C(T), specimens at different load levels and frequencies. The experimental data were initially analysed using the traditional fracture mechanics parameter $\Delta K$ which was shown to have limitations at elucidating the effects of frequency on CFCG rates in the range of 0.2–0.5 Hz. Therefore, a new fracture mechanics parameter was developed that allows these effects to be seen and accounted for more clearly. Furthermore, a new CFCG model was developed, using the introduced fracture mechanics parameter, for predicting the crack growth rates in seawater from the short-term test data in air. The proposed model has been found to correlate well with experimental data from corrosion-fatigue experiments on S355G10+M from this study and S355J2+N structural steel data available in the literature.

## 1. Introduction

The importance of global warming and the essential need for rapid emissions reduction has been widely discussed at international communities in recent years (The Intergovernmental Panel on Climate Change, 2021). One of the major actions which has been taken by various nations around the world is to use different sources of renewable energy for electricity production. Among the existing renewable energy industries, the offshore wind sector has grown significantly in the past two decades with over 7000 offshore wind turbines installed in fully commissioned offshore wind farms in 2020, as compared with less than 100 in the year 2000 (4coffshore, 2021). The Levelised Cost of Energy for offshore wind has also fallen significantly, from 190 $/MWh in 2009 to 78 $/MWh in 2019 (BloombergNEF, 2020). Offshore wind is therefore likely to play a significant role in the future of global green energy. An important issue which needs to be better understood in the design and life assessment of offshore wind turbine foundations, which are dominantly made of structural steels, is the formation of corrosion-fatigue damage and crack growth in hostile offshore environments. An improved knowledge of corrosion-fatigue will enable design optimisation for future generation of offshore wind turbine structures, helps to minimise the number of frequent inspections and also enhances the life prediction for thousands of operational offshore wind turbines around the world which is particularly critical in the context of offshore wind turbines where accessing the structures is a highly expensive process due to their remote locations.

Fatigue is a degradation mechanism in which the structures or components are damaged by receiving repeated loading cycles. Although each of the loads may be well below the level required to cause damage in isolation (i.e. below the yield stress of the material), the cumulative effect of the cyclic loading leads to the formation and propagation of cracks. Corrosion-fatigue is the process of fatigue degradation under cyclic loading conditions occurring in a corrosive environment, which can significantly accelerate the damage process. Offshore wind turbines are subjected to cyclic loading conditions due to constant exertion of the wind, wave and currents forces on the structure. Particularly at the foundations, which are subjected to higher load levels due to the application of horizontal forces on a bottom-fixed vertical structure, the seawater couples with this cyclic loading condition

* Corresponding author.
*E-mail address:* ali.mehmanparast@strath.ac.uk (A. Mehmanparast).

https://doi.org/10.1016/j.mechmat.2022.104526
Received 4 January 2022; Received in revised form 18 August 2022; Accepted 9 November 2022
Available online 11 November 2022

**Nomenclature**

| | |
|---|---|
| $a$ | Crack length |
| $a_0$ | Initial crack length |
| $a_f$ | Final crack length |
| $\left(\frac{da}{dN}\right)_{air}$ | Crack growth per cycle in air under cyclic loading condition |
| $\left(\frac{da}{dN}\right)_{I}$ | Crack growth per cycle in an inert environment under cyclic loading condition |
| $\left(\frac{da}{dN}\right)_{CF}$ | Crack growth per cycle in a corrosive environment under cyclic loading condition |
| $\left(\frac{da}{dN}\right)_{cf}$ | Cycle-dependent term that accounts for the environmental contribution below $K_{ISCC}$ |
| $\frac{da}{dt}$ | Rate of change of crack length with respect to time in a corrosive environment under static loading |
| $\left(\frac{d\bar{a}}{dt}\right)_{C}$ | Average environmental crack growth rate over one loading cycle |
| $B$ | Specimen thickness |
| BFS | Back face strain measurement technique |
| $C$ | Paris Law coefficient |
| CFCG | Corrosion-fatigue crack growth |
| C(T) | Compact tension specimen |
| CTOD | Crack Tip Opening Displacement |
| $E$ | Elastic Young's modulus |
| $f$ | Frequency |
| $f_{air}$ | Frequency in an air test |
| $f_{CF}$ | Frequency in a corrosion-fatigue test |
| $J$ | Elastic-plastic fracture mechanics parameter |
| $J_{el}$ | Elastic portion of the $J$ parameter |
| $J_p$ | Plastic portion of the $J$ parameter |
| $\dot{J}$ | Derivative of $J$ with respect to time |
| $K$ | Stress intensity factor |
| $K_{max}$ | Maximum stress intensity factor |
| $K_{min}$ | Minimum stress intensity factor |
| $K_t$ | Stress concentration factor |
| $\Delta K$ | The difference between $K_{max}$ and $K_{\min}$ |
| $\Delta\dot{K}$ | Derivative of $\Delta K$ with respect to time |
| $K_{ISCC}$ | Threshold value of $\Delta K$ in a corrosive environment |
| $m$ | Paris Law exponent |
| $N$ | Number of cycles |
| $N_f$ | Total number of cycles to failure |
| $N_i$ | Number of cycles needed for a pit to grow to a critical size |
| $N_p$ | Number of cycles needed to propagate the crack to failure |
| $P$ | Applied load |
| $P_{max}$ | Maximum applied load |
| $P_{min}$ | Minimum applied load |
| $P_{average}$ | Mean applied load |
| $P_{LC}$ | Plastic collapse load |
| $R$ | Load ratio |
| $R^2$ | Coefficient of determination in regression analysis |
| $r_p$ | Plastic zone size |
| $W$ | Specimen width |
| $Y$ | Shape function in stress intensity factor calculation |
| $\sigma$ | Stress |
| $\sigma_{0.2}$ | 0.2% proof stress |
| $\sigma_y$ | Yield stress |
| $\sigma_{\text{ref}}$ | Reference stress |
| $\varepsilon$ | Strain |
| $\varepsilon_{\text{ref}}$ | Reference strain |

resulting in corrosion-fatigue damage evolution and crack propagation which is known to be an important failure mechanism in offshore structures (Jaske et al., 1981). Therefore, the corrosion-fatigue behaviour must be accurately characterised and predicted for repair or decommission of offshore wind turbine foundations before any catastrophic failure occurs in these large-scale structures.

The aim of the present study is to comprehensively review and evaluate the limitations of existing methods for predicting CFCG behaviour in offshore steel structures and consequently develop a new approach to overcome the shortfalls of the existing models. Considering that fatigue is a cycle-dependent mechanism whereas corrosion is time-dependent, the accuracy of CFCG predictions by correlating the crack growth rate with the classic linear elastic fracture mechanics parameter, $\Delta K$, which is independent of time has been critically analysed and a new time-dependent fracture mechanics parameter has been proposed for more accurate characterisation of CFCG behaviour in steel structures. Furthermore, this time-dependent fracture mechanics apparoach has been implemented in a new model to accurately predict the corrosion-fatigue cracking behaviour of structural steels under various operational frequencies. The proposed model has been validated using corrosion-fatigue test data primarily on S355G10+M steel, carried out as a part of this study, in addition to S355J2+N data taken from the literature. Both of these sub-grades of medium strength S355 structural steel are widely used in fabrication of offshore structures, particularly offshore wind turbine foundations. The results from this study demonstrate that the life prediction of offshore steel structures can be enhanced by employing the proposed approach in life assessment procedures.

## 2. Corrosion-fatigue mechanism and existing prediction models

### 2.1. Corrosion-fatigue process

The complex process of corrosion-fatigue interaction in offshore steel structures is typically divided into four stages: surface film breakdown, pit growth, pit to crack transition and finally cracking, which includes small and then long crack growth. The first stage results in a separation of anodic and cathodic locations causing pit nucleation. Mechanical, chemical and physical factors affect this initial stage and it has been shown that a greater number of corrosion pits will form on a steel material under higher cyclic stress amplitudes (Larrosa et al., 2018). The second stage of the process, pit growth, is influenced by mechanical and chemical factors (Larrosa et al., 2018). The transition from pit evolution to crack initiation and growth is a particularly complex stage of the process. It has been shown that the point of transition is affected by the chemistry of the corrosive environment, corrosion time and stress level (Hu, 1997). The final stage of the process, which is usually referred to as corrosion-fatigue crack growth or CFCG, is the main focus of this study. Cracks resulting from the process of corrosion-fatigue are almost always transgranular, and often begin at points of raised stress, particularly corrosion pits (Larrosa et al., 2018) (Anderson, 2017). Even if an intergranular crack begins to form it will generally transform into a transgranular crack as the crack advances (Larrosa et al., 2018).

### 2.2. Corrosion-fatigue mechanisms

Depending on the material type and operational/environmental loading condition, there are a number of mechanisms which can influence fatigue initiation and propagation. Some of the important examples

of such mechanisms include: the slip bands due to plasticity accumulating at the surface, injection of vacancies due to corrosion, dynamic strain ageing, hydrogen embrittlement, hydrogen enhanced local plasticity, cold work due to fatigue cycling, low temperature creep, and intergranular attack due to stress corrosion cracking.

One mechanism proposed for driving corrosion-fatigue in offshore steel structures is that of film rupture. Based on this theory, the plastic strain induced by cyclic loading breaks the protective film (usually an oxide layer) at the crack tip, which allows for anodic dissolution of the exposed metal and hence leads to this area being corroded preferentially. There are different versions of this theory; for example, some assume that the protective film does not reform at the crack tip and hence the crack growth due to corrosion is continuous. Others assume there is reformation of the film, in which case the discontinuous nature of the crack growth may be visible via crack arrest marks on the fracture surface (Anderson, 2017). This mechanism is often referred to as anodic dissolution (Seifert et al., 2012).

Hydrogen embrittlement is another corrosion-fatigue mechanism that occurs in certain material-environment combinations. Hydrogen atoms are small, so can fit within the structure of a metallic crystal and also within grain boundaries. It is thought that the presence of hydrogen can reduce the bond strength between metal atoms, making fracture more likely (Anderson, 2017). During the oxidation of iron in the corrosion process, hydrogen is produced. The hydrogen molecules can build up and form a film on the surface of the metal, which actually inhibits the reactions and slows down corrosion (also known as polarisation) (Venzlaff et al., 2013). However, if oxygen is present, it can react with the hydrogen in the film and produce water, in a process called oxygen depolarisation (Li et al., 1984). This reduces the protection of the metal and accelerates the corrosion process.

High strength steels have been found to be particularly vulnerable to hydrogen embrittlement, and the influence of the environment during corrosion-fatigue is primarily due to this mechanism in such steels (Li et al., 1993) (Weng et al., 2013). It has been shown that medium strength steels in an NaCl solution experience all three of these corrosion fatigue mechanisms; anodic dissolution, hydrogen embrittlement and oxygen depolarisation (Li et al., 1993) (Chatterjee and Singh Raman, 2011).

### 2.3. Corrosion-fatigue crack growth behaviour types

The corrosion-fatigue crack growth behaviour in various engineering materials can be divided into three general types which are schematically shown in Fig. 1 (McEvily and Wei, 1972). As shown in Fig. 1(a), in Type A the CFCG process starts at lower values of stress intensity factor, $K$, that in the inert (i.e. air) case, and for a given value of $K$ higher crack growth rates are expected in the primary and secondary (also known as the Paris region) crack growth regions compared to the inert environment. In Type B CFCG behaviour (see Fig. 1(b)), the crack growth rate is aligned with the inert case up until some threshold, denoted $K_{ISCC}$, and beyond this a substantial increase in crack growth rate occurs. The final CFCG behaviour, Type C, is a combination of Type A and Type B behaviours where higher crack growth rates, compared to the inert environment, are expected throughout the entire range of $K$ values with a further increase taking place for values equal to or higher than $K_{ISCC}$ (McEvily and Wei, 1972).

High strength steels often exhibit substantial stress corrosion cracking under sustained static loading in a corrosive environment due to hydrogen embrittlement (Chatterjee and Singh Raman, 2011). Medium strength steels can also exhibit some degree of stress corrosion cracking in an NaCl solution typically due to a combination of hydrogen embrittlement and anodic dissolution (Chatterjee and Singh Raman, 2011). Therefore, as some degree of environmentally assisted sustained load crack growth would be expected, medium strength steels in seawater are likely to exhibit Type B or C behaviour.

### 2.4. Existing corrosion-fatigue crack growth models

#### 2.4.1. Original linear superposition model

The first model for describing the crack growth rate of metals in a corrosive environment under cyclic loading condition was developed by Wei and Landes (1969). In this CFCG approach, which is commonly referred to as the 'linear superposition model', it is assumed that the total crack growth rate in a corrosive environment is the sum of a mechanically dependent 'fatigue' term and an environment dependent 'corrosion' term:

$$\left(\frac{da}{dN}\right)_{CF} = \left(\frac{da}{dN}\right)_{I} + \int \frac{da}{dt}(K)dt \tag{1}$$

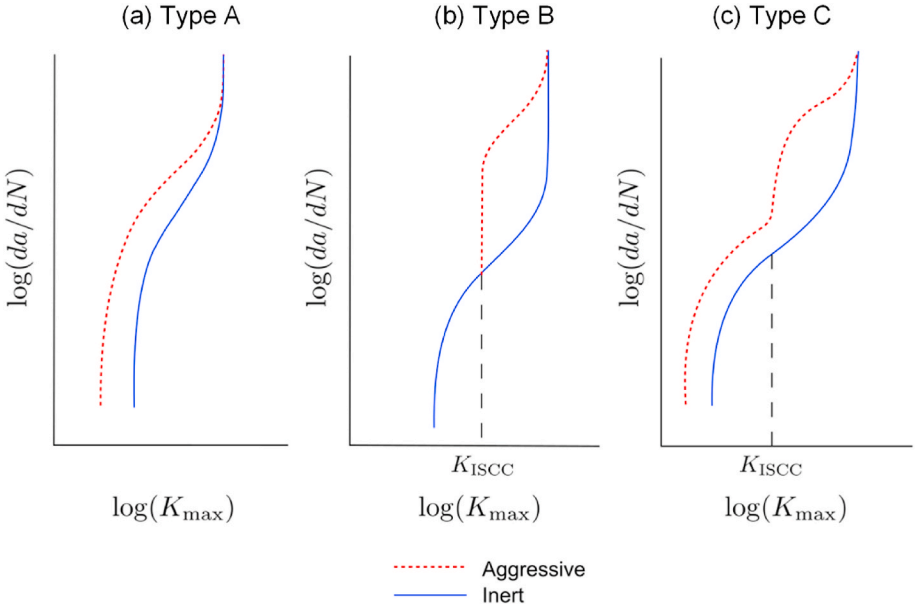


**Fig. 1.** Different types of corrosion-fatigue cracking behaviour: (a) Type A, (b) Type B, (c) Type C.

where $\left(\frac{da}{dN}\right)_{CF}$ is the CFCG rate, $\left(\frac{da}{dN}\right)_{I}$ is the crack growth rate in an inert environment under cyclic loading and $\frac{da}{dt}$ is the crack growth rate in a corrosive environment under static loading which is a function of the stress intensity factor, $K$.

The integral term in Equation (1) describes the crack growth over one cycle due to sustained load crack growth in a corrosive environment. McEvily and Wei suggested that the linear superposition model is well suited to describe Type B corrosion-fatigue behaviour, as it can account of the $K_{ISCC}$ threshold for a corrosive environment (McEvily and Wei, 1972).

#### 2.4.2. Variants of superposition model

Wei further developed the superposition model by including an additional term to the original linear superposition model (Wei, 1978):

$$\left(\frac{da}{dN}\right)_{CF} = \left(\frac{da}{dN}\right)_{I} + \left(\frac{da}{dN}\right)_{cf} + \int \frac{da}{dt}(K)dt \tag{2}$$

where $\left(\frac{da}{dN}\right)_{cf}$ is a cycle-dependent term that accounts for the environmental contribution below $K_{ISCC}$. The addition of this term extended the applicability of the model to some Type C material-environment systems. Wei and Simmonds suggested later that this additional term arises from the reaction of the corrosive medium with new cracks on the surface and depends on the degree of reaction during a single cycle (Wei and Simmons, 1981). They also noted that in many practical engineering situations, materials would be selected that had minimal vulnerability to crack growth under static or sustained loading. Hence the $\frac{da}{dt}$ term would be negligible in many of such cases, whilst the new $\left(\frac{da}{dN}\right)_{cf}$ term would be more significant.

Another variant of the superposition model was built by Wei and Gao (1983) in which the CFCG rate is defined as:

$$\left(\frac{da}{dN}\right)_{CF} = \left(\frac{da}{dN}\right)_{I}(1-\varphi) + \left(\frac{da}{dN}\right)^{*}_{cf,s}\varphi + \left(\frac{da}{dN}\right)_{SCC} \tag{3}$$

where $\left(\frac{da}{dN}\right)^{*}_{cf,s}$ is the pure corrosion-fatigue rate, $\left(\frac{da}{dN}\right)_{SCC}$ is the contribution to crack growth per cycle from sustained-load crack growth in a corrosive environment, and $\varphi$ is the fractional area of crack that is undergoing pure corrosion-fatigue.

Based on the superposition approach, there are three equations proposed in by Anderson (2017) to describe the CFCG behaviour for Types A, B and C material-environment combinations which are shown in Equations (4)–(6), respectively.

$$\left(\frac{da}{dN}\right)_{CF} = \varphi\left(\frac{da}{dN}\right)_{I} \tag{4}$$

$$\left(\frac{da}{dN}\right)_{CF} = \left(\frac{da}{dN}\right)_{I} + \frac{1}{f}\left(\frac{d\bar{a}}{dt}\right)_{C} \tag{5}$$

$$\left(\frac{da}{dN}\right)_{CF} = \varphi\left(\frac{da}{dN}\right)_{I} + \frac{1}{f}\left(\frac{d\bar{a}}{dt}\right)_{C} \tag{6}$$

where $\left(\frac{d\bar{a}}{dt}\right)_{C}$ is the average environmental crack growth rate over one loading cycle and $f$ is the loading frequency. In the Type C model (see Equation (6)), at low frequencies the corrosion term will be dominant, whereas at high frequencies the corrosion per cycle will be negligible. It has been stated in (Anderson, 2017) that Type A material-environment combinations are time-independent, unlike Type B and C. However, this is not always the case and a time dependency can be present in Type A.

It has been shown in the literature that the calculation of the fractional area $\varphi$ is not straightforward (Li et al., 1984) (Wei and Simmons, 1981). Also, as Kim et al. noted in their review of quantitative CFCG models, to employ the superposition model the crack growth rate $da/dt$ under sustained loading in a corrosive environment must be known as a function of the stress intensity factor (Kim et al., 1998). For the vast majority of material-environment systems this relationship is not typically known and is difficult to identify (Kim et al., 1998). Therefore, it is generally hard to calibrate the original and variants of the superposition model to predict CFCG rate for engineering materials.

#### 2.4.3. Process competition model

Another fundamentally different model to that of the superposition was developed by Austen and Walker, which is commonly referred to as the 'process competition model' (Austen and Walker, 1977). The idea behind this model is that the processes of fatigue and corrosion are competitive, and that the crack growth rate will be equal to the fastest available rate. The updated version of this model, which was presented in (Austen and Mcintyre, 1979), allowed for the accounting of waveform affects; however, it was found out that the competition model could result in significant errors when predicting the CFCG behaviour of some types of steels.

#### 2.4.4. Cycle-dependent models

Another approach to predict the total number of cycles to failure in a corrosion-fatigue system is using the damage accumulation corrosion-fatigue models. An example of such models is that of developed by Wang et al. where it is assumed that a stable crack will initiate from a corrosion pit once it reaches a critical size at a given load level (Wang et al., 2001). The model is based on estimating the total number of cycles to failure, $N_f$, by the following sum:

$$N_f = N_i + N_p \tag{7}$$

where $N_i$ is the number of cycles needed for a pit to grow to a critical size and $N_p$ is the number of cycles needed to propagate the crack to failure. In this approach, it is often assumed that the corrosion pit is a semi-circular geometry with the pit size, $a_p$, defined as a function of the cube root of time, as shows by Kondo (1989). Using this approach, the critical pit size at which the crack starts to propagate can be predicted.

Once $N_i$ is predicted in Equation (7), the number of cycles for the crack to propagate to failure, $N_p$, is then simply calculated via the Paris Law:

$$\frac{da}{dN} = C(\Delta K)^m \tag{8}$$

where $\Delta K$ is the stress intensity factor range (i.e. the difference between $K_{max}$ and $K_{min}$), and $C$ and $m$ are the Paris Law constants.

By assuming that $N_p$ can be divided into two terms which represent the number of cycles to propagate a short crack to a long crack and the number of cycles to propagate a long crack to the final crack length $a_f$ which is the point of failure, the number of cycles to propagate a crack from length $a_1$ to $a_2$ can be described as:

$$N = \int_{a_1}^{a_2} C(\Delta K)^m = \int_{a_1}^{a_2} C\left(\beta K_t \Delta\sigma\sqrt{\pi a}\right)^m \tag{9}$$

where $\Delta\sigma$ is the stress range, $a$ is the crack length, $K_t$ is the stress concentration factor, $\beta = 2.2/\pi$ for a semi-circular flaw and $\beta = 1$ for a through crack. Using this approach, it is assumed that the same Paris Law constants $C$ and $m$ are applicable for both the short and long crack regimes.

There are a number of issues with the assumptions underpinning the cycle-dependent life prediction approach. It is unclear whether the use of the fracture mechanics parameter is appropriate for several reasons. As noted by Fatoba in 2016, fracture mechanics parameters are obtained from pre-cracked specimens, whereas some pits initiate on smooth surfaces and pitting may induce local plasticity hence drawing further questions about the applicability of a linear-elastic fracture mechanics parameter (Fatoba, 2016). Additionally, the pit size is assumed to be a function of corrosion-related parameters only and yet it is recognised

that the rate of pit growth also depends on mechanical factors such as the degree of plasticity (Larrosa et al., 2018). The model also treats the pit as a semi-circular flaw and therefore implicitly assumes that the crack will initiate from the base of the pit. However, Fatoba found that in many cases cracks in fact initiate from the mouth of pits (Fatoba, 2016). Finally, the approach taken to calculate $N_p$ is entirely based on fatigue theory and assumes no contribution from the corrosive environment while many material-environment combinations exhibit accelerated crack growth rate in the latter stages of the corrosion-fatigue process. Therefore, there are some significant inaccuracies involved in prediction of corrosion-fatigue using the modelling approaches which are based on the cycle-dependent damage analysis (e.g. (Sriraman and Pidaparti, 2009) (Li and Akid, 2013) (Kalnaus et al., 2011) (Menan and Henaff, 2009)).

#### 2.4.5. Other models available in the literature

In addition to the well-established corrosion-fatigue life prediction models mentioned above, a number of other novel approaches for corrosion-fatigue modelling have been developed by various researchers in recent years. Some notable examples of such recent methods which have been developed for a range of different industrial applications are: the use of short crack growth models for corrosion-fatigue life estimation proposed by Chapetti and implemented by Larrosa (Larrosa et al., 2016), a new life assessment approach based on a microstructural short crack growth model by Balbin (Balbín et al., 2021), the use of cohesive zone models proposed by R. Fernández-Sousa (Fernández-Sousa et al., 2022), and a Cellular Automaton Finite Element (CAFE) model for pit development under corrosion-fatigue conditions developed by Fatoba et al. (2018).

### 2.5. Frequency effects on corrosion-fatigue behaviour

A review of the corrosion-fatigue models presented above shows that this process is often broadly split into two stages, with the first including surface breakdown and pit formation and growth, and the second consisting of crack propagation. Researchers often consider the former of these stages to be corrosion dominated, and the latter mechanically dominated, as explained by Larrosa et al. in their review of corrosion-fatigue models (Larrosa et al., 2018). Although this broad categorisation may be valid, the question remains about how to interpret this appropriately into corrosion-fatigue modelling. It is clear that the non-dominant process often still plays an important role, for example, higher stress values can lead to a greater number of corrosion pits forming in the earlier stages (Larrosa et al., 2018). One result of this assumption is that some researchers have implemented corrosion-fatigue models that consider the latter stage of the process to be entirely mechanically dominated, with no influence from the corrosive environment (e.g. (Wang et al., 2001) (Sriraman and Pidaparti, 2009) (Li and Akid, 2013)). However, experimental investigations of the effect of frequency on crack growth rate in corrosion-fatigue experiments have demonstrated clear limitations to this approach.

It is well known that in an inert environment, frequency has little to no effect on the crack growth rate (Anderson, 2017). However, the introduction of a corrosive environment introduces a frequency dependency in many material-environment combinations. This is particularly important by considering that the realistic impact of corrosive environments on the fatigue crack growth behaviour of materials will be only revealed when the CFCG tests are performed at relatively low frequencies where the time-dependent corrosion mechanism will have sufficient time to interact with fatigue mechanism. It is worth considering that depending on the test frequency in CFCG experiments, the cracking behaviour of the material can be dominated by fatigue, corrosion or combined corrosion-fatigue interaction. While the corrosion process will become more pronounced at lower frequencies, if the CFCG tests are performed at sufficiently high frequencies the fatigue crack growth results are expected to fall upon the inert (i.e. air) data as the time-dependent corrosion process will not play a substantial role in the cracking behaviour of the material and the advancement of the crack will be dominantly caused by fatigue.

Etris et al. investigated the impact of a wide range of factors on CFCG rate in AISI 4340 steel and found that for a given value of $\Delta K$ the crack growth rate was substantially increased in water as compared with Argon, and to a much greater extent at 0.5 Hz compared to 5.0 Hz (Etris et al., 1973). Vosikovsky conducted experiments on X-65 pipeline steel and demonstrated that the crack growth rate was 10 times faster in salt water at 0.01 Hz than in air and a decrease in the loading frequency substantially increased the CFCG rate (Vosikovsky, 1975). It is typically seen for many material-environment combinations that the effect of frequency is only present for sufficiently low frequencies. For example, Yu et al. studied the effect of loading frequency on crack growth rate in humid air on 7N01 aluminium alloy (Yu et al., 2020) and found an elevated crack growth rate at 0.1 Hz, whilst that the rates at 1 Hz and 10 Hz were almost identical. Similarly, Anderson showed the impact of frequency on Inconel 600 in a high temperature NaOH solution where the crack growth rate decreased with increasing frequency before levelling off at those tests conducted above 1 Hz (Anderson, 2017).

### 2.6. The fracture mechanics parameter $\Delta K$

Another result of the assumption that corrosion-fatigue is dominated by one process depending on the stage of development, is that the vast majority of corrosion-fatigue models that are developed to predict the crack propagation behaviour of materials use the fracture mechanics paramete $\Delta K$ (Larrosa et al., 2018). Adedipe et al. conducted corrosion-fatigue experiments on S355J2+N steel in seawater and showed that, other than at low values of $\Delta K$, under the same loading condition there is generally a greater crack growth rate in the seawater tests, conducted at various frequencies, compared with the experiments conducted in air (Adedipe et al., 2015). The frequencies studied in the corrosion-fatigue tests were of a small range including 0.3 Hz, 0.35 Hz and 0.4 Hz. From the traditional correlation of the crack growth rate with $\Delta K$ in (Adedipe et al., 2015) it is difficult to pull out any consistent correlation between the cracking rate and the test frequency. However, the question could be raised about whether this could be influenced by the use of the fracture mechanics parameter $\Delta K$. This parameter was originally designed to characterise the elastic stress distributions near the crack tip and later on was employed to build a correlation with the crack growth rates under cyclic loading with no accounting for environmental factors. The frequency (hence time-dependence) effects seen in the crack propagation stages of corrosion-fatigue are a result of the environmental influences. Since the extended application of $\Delta K$ in characterisation of fatigue crack propagation was not designed for considering environmental effects, it may be concluded that for small changes in frequency, it is too blunt a tool to fully capture the impact of these small changes on crack growth rates. Xin and Veljkovic explored the use of other parameters for the use of tracking the behaviour of crack growth rates under corrosion-fatigue conditions (Xin and Veljkovic, 2020). They plotted the crack growth rate against the $J$-integral and also against the Crack Tip Opening Displacement (CTOD). Although the use of the $J$-integral parameter introduces considerations of plasticity, both are still fracture mechanics parameters unrelated to the process of corrosion.

### 2.7. Motivation for present study

The review of the existing CFCG models shows that many existing corrosion-fatigue models can be difficult to apply in practice as they largely rely on the use of empirical data from the case of static loading in a corrosive environment while such data are not typically available in the literature (Kim et al., 1998). Moreover, there is limited exploration of the use of alternative parameters to $\Delta K$ to model the later stages of the corrosion-fatigue process. As explained before, the fracture mechanics

parameter $\Delta K$ was not designed to account for environmental effects and may not be sensitive to small changes in frequency during corrosion-fatigue tests. Despite this, $\Delta K$ is still used in the vast majority of corrosion-fatigue models that examine the crack propagation stage of the process. This study will therefore develop a new model for predicting corrosion-fatigue behaviour at the crack propagation stage from the inert case, that does not require data from the case of static loading in a corrosive environment. The model will use a new time-dependent fracture mechanics parameter and will account for environmental effects. The present study is supported by experimental investigation of CFCG behaviour in structural steels at a small range of frequencies to validate the proposed prediction model.

## 3. Materials and methods

### 3.1. Material

A type of steel which is most commonly used in offshore wind structures is EN10025 S355 (Igwemezie et al., 2019). The subgrade studied in this research is S355G10+M, which is typically used in critical joints, and hence is crucial to the corrosion-fatigue performance of the structures (Igwemezie and Mehmanparast, 2020). The 'G10' indicates a subgrade with particular treatment to ensure a fine grain microstructure. The 'M' indicates that the subgrade has been thermo-mechanical control rolled. The chemical composition of S355G10+M steel used in this study is shown in Table 1.

### 3.2. Experimental set-up

The corrosion-fatigue experiments in this study were conducted on compact tension, C(T), specimens in accordance with ASTM E647 (ASTM International, 2015) and analysed using the guidelines in BS 7910 (British Standard, 2019). The specimens were pre-cracked in air via the $K$-decreasing method as recommended by ASTM E647 (ASTM International, 2015). Test IDs were given of the form "Px-Fy" where x = 9 or 10 kN refers to the maximal load applied during the corrosion-fatigue tests and y = 0.2, 0.3 or 0.5 Hz refers to the test frequency. All C(T) specimens had the width of $W = 50$ mm, thickness of $B = 16$ mm and the initial crack length of approximately $a_0 = 22$ mm after pre-cracking and at the beginning of the CFCG tests. The cyclic loading condition was applied using a sinusoidal wave in each experiment with a load ratio (i.e. the ratio of minimum to maximum load in a cyclic test) of $R = 0.1$. Six CFCG tests were performed in free corroding conditions, half of which under the maximum load of $P_{max} = 9$ kN whereas the other three were tested under $P_{max} = 10$ kN. For each set of these tests, three different frequencies of $f = 0.2$, 0.3 and 0.5 Hz were applied. Additionally, two fatigue crack growth tests were performed in air under $P_{max}$ of 9 and 10 kN using an $R$ ratio of 0.1 at 5 Hz. The air tests were performed under the same loading condition as the CFCG tests for comparison purposes. Moreover, the results from the air tests were used to derive calibration curves for crack growth monitoring in CFCG experiments, the details of which are explained below.

Prior to commencement of the corrosion-fatigue experiments, the specimens were immersed in artificial seawater, prepared according to ASTM D1141 (ASTM International, 2021) for 48 h. The specimens were kept submerged throughout the experiment and the pH was kept between 8.0 and 8.2 while the temperature of the seawater was maintained between 7.5°C and 8.2°C, to simulate the North Sea conditions. The seawater was kept in motion by a pump at a rate of approximately 4 L/min. At the end of the tests the specimens were soaked in liquid nitrogen and fracture opened in order to measure the final crack length.

**Table 1**
Chemical composition of S355G10+M steel.

| Element | C | Mn | Ni | Si | Cu | Cr | Mo |
|---|---|---|---|---|---|---|---|
| Percentage | 0.06 | 1.57 | 0.33 | 0.27 | 0.24 | 0.03 | 0.01 |

The crack growth monitoring in CFCG tests was conducted using the back face strain (BFS) measurement technique. For this purpose, a strain gauge was attached to the back face (i.e. at the mid-height and mid-thickness) of the C(T) specimens and the bending strain was continuously monitored throughout the CFCG tests. The full details of the crack growth monitoring in CFCG tests using the BFS technique can be found in (Mehmanparast et al., 2018). The crack lengths were then calculated via the calibration curves obtained from the tests in air on nominally identical samples using which the BFS values were correlated with the crack lengths for the same loading conditions examined in CFCG tests. The calibration curves were derived from the two fatigue experiments conducted in air at the maximum load levels of 9 and 10 kN which are shown in Fig. 2. In these calibration air tests a strain gauge measured the bending strain at the back of the specimens while digital cameras were used to measure the crack length.

### 3.3. Data analysis method

The crack growth rate, $da/dN$, was calculated via the incremental polynomial method with a seven-point fit in accordance with BS EN ISO 11782 (British Standard, 2008). For each crack length $a_i$, calculated using the BFS method, a quadratic polynomial fit was made to the set of 7 points $(a_{i-3},N_{i-3})$, …., $(a_{i+3},N_{i+3})$. The derivative of this polynomial at $N_i$ was taken as $da_i/dN_i$. The fatigue crack growth rates obtained from the tests were correlated with the linear elastic fracture mechanics parameter $\Delta K$ which was calculated using the following equation:

$$\Delta K = \frac{P_{max} - P_{min}}{B\sqrt{W}} Y\left(\frac{a}{W}\right) \tag{10}$$

where $P_{max}$ is the maximum applied load, $P_{min}$ is the minimum applied load, and $Y\left(\frac{a}{W}\right)$ is a geometry dependent shape function the solutions of which for various standard cracked geometries can be found in ASTM E647 (ASTM International, 2015). The power-law correlation between $da/dN$ and $\Delta K$ in the secondary fatigue crack growth region is often referred to as the Paris Law (see Equation (8)).

The elastic-plastic fracture mechanics parameter, $J$, was calculated using the reference stress approach in the present study. The Poisson's ratio was taken as $\nu = 0.3$ and the elastic Young's modulus as $E = 196$ GPa, as reported by Jacob et al. for S355G10+M structural steel (Jacob et al., 2018). The plastic strain data for S355G10+M base metal was also taken from Jacob et al. (2018). It is worth noting that the material used in this study was from the same batch that was previously characterised

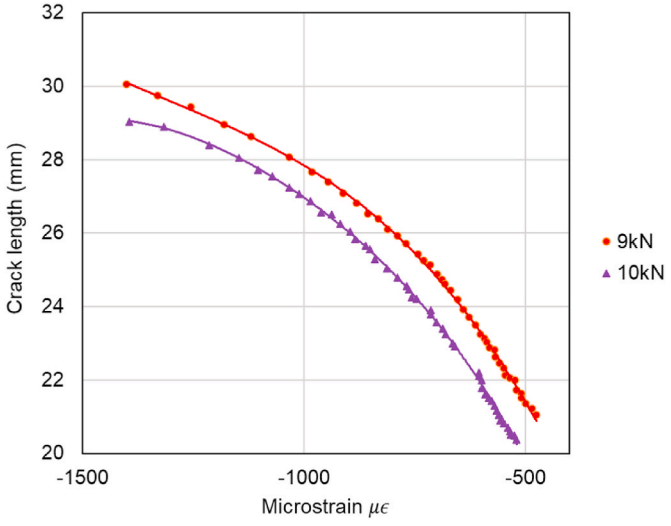


**Fig. 2.** Back face strain calibration curves obtained from air tests on S355G10+M steel C(T) specimens with the maximum load of 9 kN and 10 kN.

by Jacob et al. (2018). The Ramberg-Osgood material model (see Equation (11)), the constants of which are employed in $J$ calculations using the reference stress approach, was then fit to elastic-plastic tensile data and a line of best fit was made using the least squares algorithm employed in MATLAB.

$$\varepsilon = \frac{\sigma}{E} + A\sigma^N \tag{11}$$

In Equation (11), $\varepsilon$ is the total strain, $\sigma$ is the stress, $E$ is the elastic Young's modulus, and $A$ and $N$ are Ramberg-Osgood material model constants which were found to be $A = 2.65 \times 10^{-23}$ and $N = 7.76$ for S355G10+M structural steel.

The reference stress, $\sigma_{ref}$, was calculated using the following equation (Mehmanparast, 2012):

$$\sigma_{ref} = \frac{\sigma_{0.2} P}{P_{LC}} \tag{12}$$

where $P$ is the applied load, $\sigma_{0.2}$ is 0.2% proof stress (which is 455 MPa for S355G10+M structural steel), and $P_{LC}$ is the plastic collapse load which can be calculated for C(T) specimen geometry with plane strain condition using the following equation (Mehmanparast, 2012):

$$P_{LC} = \left( \sqrt{2.702\left(1 + 1.702\left(\frac{a}{W}\right)^2\right)} - \left(1 + 1.702\left(\frac{a}{W}\right)\right) \right) \frac{2}{\sqrt{3}} B_n W \sigma_{0.2} \tag{13}$$

where $B_n$ is the specimen net thickness between side grooves which, which in this case is equal to $B$ since there was no side groves in the test specimens. The normalised reference stress $\sigma_{ref}/\sigma_{0.2}$ is commonly used to assess the extent of plasticity in cracked geometries (Mehmanparast, 2012). If this ratio is below one it indicates limited plasticity while the values of much greater than unity imply widespread plasticity in the cracked geometry.

The $J$ parameter based on the reference stress approach was then calculated as the sum of the elastic component of $J$, $J_{el}$, and plastic component of $J$, $J_p$, using the following equations:

$$J = J_{el} + J_P \tag{14}$$

$$J_{el} = \frac{K^2}{E'} \tag{15}$$

$$J_p = \mu \sigma_{ref} \left(\varepsilon_{ref} - \frac{\sigma_{ref}}{E}\right) \left(\frac{K}{\sigma_{ref}}\right)^2 \tag{16}$$

where $\mu = (1 - \nu^2)$ for plane strain condition ($\mu = 1$ for plane stress condition), and $E'$ is the effective Young's modulus which is equal to $E' = E/(1\text{-}\nu^2)$ for plane strain condition ($E' = E$ for plane stress condition). In Equation (16), the reference strain, $\varepsilon_{ref}$, was calculated by taking the value of strain corresponding to the reference stress value according to the Ramberg-Osgood material model (Equation (11)).

The time derivatives of $J$ and $\Delta K$, denoted $\dot{J}$ and $\dot{\Delta K}$, were calculated using the seven-point incremental polynomial method which was previously employed to calculate $da/dN$ as described in BS EN ISO 11782 (British Standard, 2008).

The plastic zone size, $r_p$, was estimated using the following equation (Mehmanparast, 2012):

$$r_p = \frac{1}{\beta_1 \pi} \left(\frac{N-1}{N+1}\right) \left(\frac{K}{\sigma_y}\right)^2 \tag{17}$$

where $\beta_1 = 3$ for plane strain conditions ($\beta_1 = 1$ for plane stress), $N$ is the power-law hardening exponent in Ramberg-Osgood material model (taken as $N = 7.76$ for S355G10+M structural steel), and $\sigma_y$ is the yield stress of the material (taken as 455 MPa for S355G10+M structural steel (Jacob et al., 2018)).

## 4. Test results and discussion

### 4.1. Crack growth rate versus $\Delta K$ and Paris Law fits

The results of the corrosion-fatigue experiments, presented in the form of traditional $da/dN$ vs. $\Delta K$ curves in log-log axes, are shown in Fig. 3(a) and (b) for the maximum load levels of 9 kN and 10 kN, respectively. Also included in these figures are the results from the air tests performed under the same loading condition. The effect of the corrosive environment is evident in these figures as the crack growth rate is clearly greater than the inert case, particularly in the case of the 9 kN maximum load. The effect of test frequency on the cracking behaviour in CFCG experiments, however, is less evident. As discussed in Section 2.3, Type B or C behaviour would be expected for medium strength steel in seawater. Fig. 3 shows that there is no significant increase in crack growth rate above some threshold $K_{ISCC}$, suggesting Type C behaviour is present without a significant contribution from environmentally assisted sustained load crack growth.

Fig. 4(a) and (b) show the Paris Law fits applied to the linear (i.e. secondary region) portion of the trends in log-log axes. The Paris Law constants, $C$ and $m$ values (see Equation (8)), from these one-stage regression fits together with the coefficients of determination, $R^2$, are summarised in Table 2. It has been explained in BS 7910 (British Standard, 2019) that a simplified one-stage power-law fit is not always appropriate to describe the fatigue crack growth behaviour of engineering materials (British Standard, 2019). In the present study, two-stage power-law trends have been found more appropriate for P9–F0.5, P10–F0.2, P10–F0.3 and P10–F0.5 CFCG tests due to the slope change in the trends at lower values of $\Delta K$. The two-stage fits for these tests are shown in Fig. 5 and the two-stage power-law constants (Stage A for lower $\Delta K$ region and Stage B for higher $\Delta K$ region) are summarised in Table 3.

The general observation from these graphs implies that the frequency change in corrosion-fatigue tests may result in some changes in the cracking rate, but the exact extent of this change in the crack growth trend depends on the load level, $\Delta K$ range and level of scatter in the data. The tests conducted at 0.5 Hz in particular appear to display a lower crack growth rate than those at 0.2 and 0.3 Hz for $\Delta K$ of less than 25.5 $MPa\sqrt{m}$ for the 9 kN tests and 23.0 $MPa\sqrt{m}$ for the 10 kN tests. It has been found elsewhere in the literature that the environmental contribution is often starker at lower values of $\Delta K$ (Fatoba, 2016) (Menan and Henaff, 2009). In the 10 kN tests, the trends of the 0.2 and 0.3 Hz tests appeared very similar. In the 9 kN tests, the 0.3 Hz test appeared to have the greatest crack growth rate. However, as can be seen from Fig. 4(a), P9–F0.3 test had the greatest scatter and also the lowest $R^2$ value in Table 2. There were also some unusually high crack growth rate values observed at low values of $\Delta K$, which might be associated with the corrosion damage build up ahead of the crack tip and slow crack initiation from the existing pre-crack.

### 4.2. Crack growth analysis using alternative fracture mechanics parameters

It may be that the fracture mechanics parameter $\Delta K$ is not the most appropriate parameter to elucidate the effects of frequency within this relatively small range of 0.2–0.5 Hz in CFCG tests. The use of other parameters is therefore explored in this section by plotting the crack growth rate against several other fracture mechanics parameters including $K_{max}$, the elastic portion of the $J$ parameter $J_{el}$, and the total $J$ parameter in Fig. 6, Figs. 7 and 8, respectively. As explained earlier in Section 3.3, the reference stress method was used in this study to calculate the $J$ parameter.

The CFCG trends observed in Figs. 6 and 7 appear similar to those previously explored using the traditional crack growth rate vs. $\Delta K$ graphs shown in Fig. 3. In particular, the effect of frequency has not been

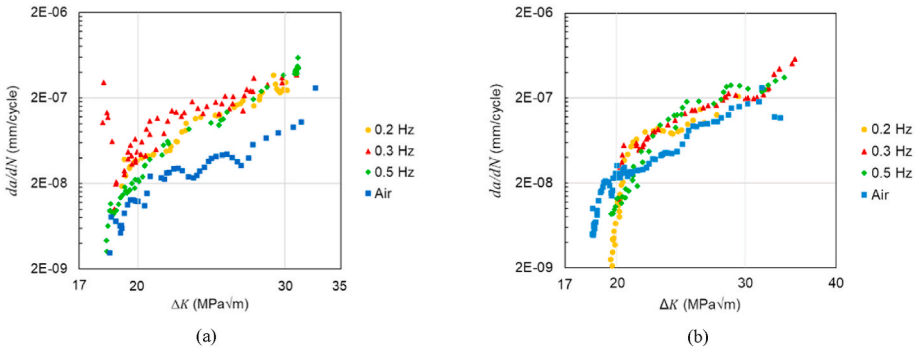


**Fig. 3.** Crack growth rate vs. $\Delta K$ for the tests on S355G10+M steel samples under (a) 9 kN, and (b) 10 kN maximum load.

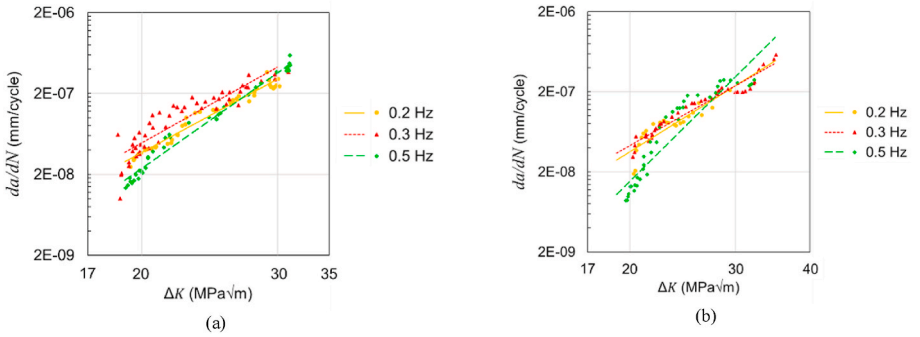


**Fig. 4.** One-stage Paris Law fits for CFCG tests on S355G10+M steel samples under (a) 9 kN, and (b) 10 kN maximum load.

**Table 2**
One-stage Paris Law parameters for CFCG tests on S355G10+M steel samples.

| | P9–F0.2 | P9–F0.3 | P9–F0.5 | P10–F0.2 | P10–F0.3 | P10–F0.5 |
|---|---|---|---|---|---|---|
| $C$ | $7.28 \times 10^{-15}$ | $5.80 \times 10^{-15}$ | $4.49 \times 10^{-17}$ | $2.98 \times 10^{-14}$ | $1.33 \times 10^{-13}$ | $3.71 \times 10^{-18}$ |
| $m$ | 5.16 | 5.33 | 6.71 | 4.67 | 4.23 | 7.39 |
| $R^2$ | 0.916 | 0.878 | 0.973 | 0.868 | 0.909 | 0.728 |

made any clearer by using these three fracture mechanics parameters. The relationship between $\Delta K$ and $K_{max}$ in Equation (18) shows that for a fixed value of $R$ ratio (i.e. $R = 0.1$ in this case) these two parameters are linearly proportional to each other. Similarly, as shown previously in Equation (15), $J_{el}$ is proportional to the stress intensity factor to the second power. Therefore, it is unsurprising that $K_{max}$ and $J_{el}$ do not draw out the frequency effects better than $\Delta K$ as they are both rescaled versions of $\Delta K$.

$$\Delta K = K_{max} - K_{min} = (1 - R)K_{max} \tag{18}$$

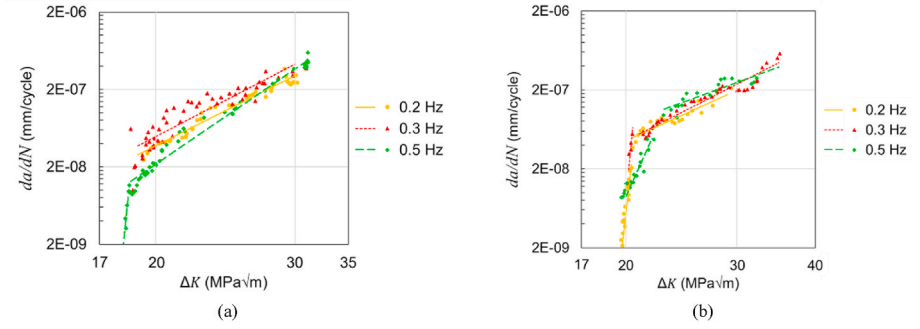


**Fig. 5.** One-stage or two-stage power-law fits for CFCG tests on S355G10+M steel samples under (a) 9 kN, and (b) 10 kN maximum load.

**Table 3**
Two-stage power-law parameters for CFCG tests on S355G10+M steel samples.

| | P9–F0.5 | | P10–F0.2 | | P10–F0.3 | | P10–F0.5 | |
|---|---|---|---|---|---|---|---|---|
| | Stage A | Stage B | Stage A | Stage B | Stage A | Stage B | Stage A | Stage B |
| $C$ | $7.01 \times 10^{-136}$ | $1.69 \times 10^{-17}$ | $4.21 \times 10^{-103}$ | $8.81 \times 10^{-13}$ | $3.98 \times 10^{-117}$ | $2.30 \times 10^{-13}$ | $6.52 \times 10^{-32}$ | $1.19 \times 10^{-11}$ |
| $m$ | 100 | 7.00 | 72.3 | 3.62 | 83.3 | 4.07 | 17.8 | 2.92 |
| $R^2$ | 0.954 | 0.974 | 0.870 | 0.873 | 0.888 | 0.896 | 0.956 | 0.816 |

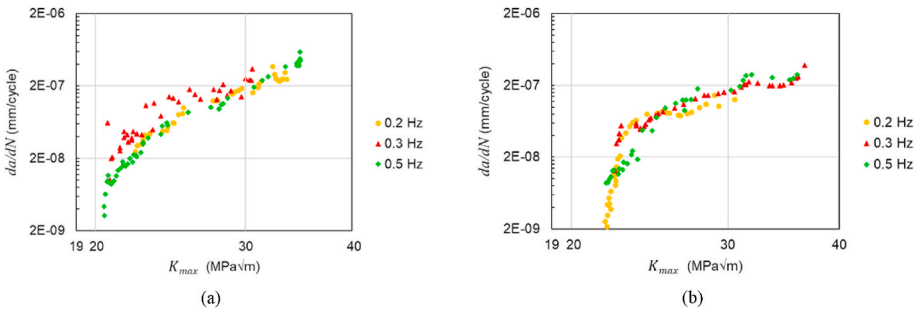


**Fig. 6.** Crack growth rate vs. $K_{max}$ for CFCG tests on S355G10+M steel samples under (a) 9 kN, and (b) 10 kN maximum load.

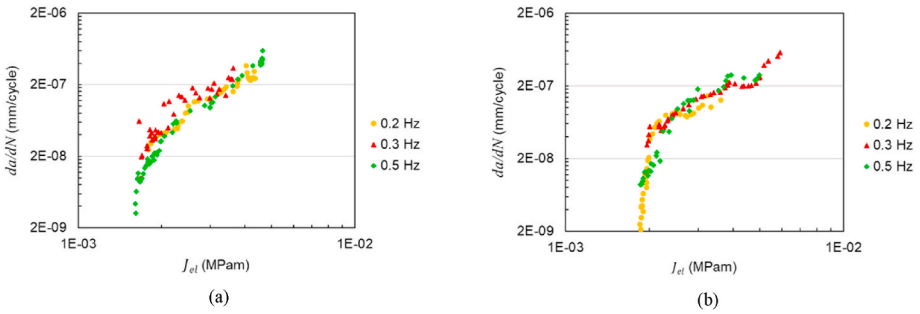


**Fig. 7.** Crack growth rate vs. $J_{el}$ for CFCG tests on S355G10+M steel samples under (a) 9 kN, and (b) 10 kN maximum load.

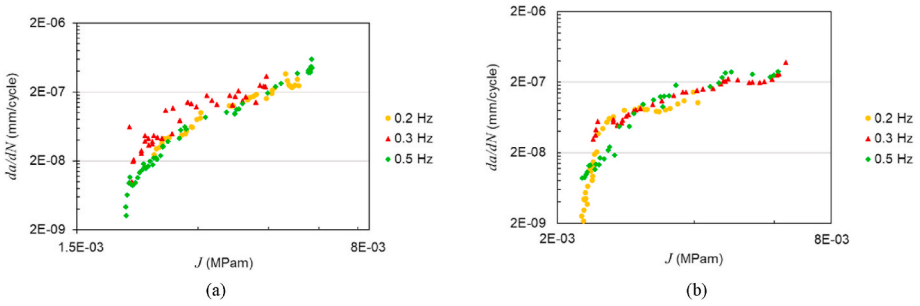


**Fig. 8.** Crack growth rate vs. $J$ for CFCG tests on S355G10+M steel samples under (a) 9 kN, and (b) 10 kN maximum load.

It can be seen in Figs. 7 and 8 that the graphs with $J_{el}$ and $J$ on the x-axis both look very similar when these fracture mechanics parameters are correlated with the crack growth rate. This suggests that there may be limited plasticity in these experiments, hence the plastic component of $J$ parameter $J_p$ (see Equation (14)) is negligible. The degree of plasticity is explored and discussed further in Section 4.4 in which the appropriateness of the $J$ parameter in characterisation of the fatigue crack growth behaviour of the material has been discussed in more detail. All the fracture mechanics parameters examined so far ($\Delta K$, $K_{max}$, $J_{el}$ and $J$) only depend on the specimen dimensions, geometry, crack length, loading conditions and material properties and none of them is dependent on any aspect of the corrosion mechanism. Therefore, it is unsurprising that the effects of frequency are not any clearer using the alternative fracture mechanics parameters compared with the use of the traditional $\Delta K$ parameter.

### 4.3. New time-dependent corrosion-fatigue parameters

As clearly established in the literature, fatigue is a cycle-dependent phenomenon, whereas corrosion is time-dependent (Larrosa et al., 2018). The combination of corrosion and fatigue generally retains some degree of time dependency when the frequency is sufficiently low, as explained in Section 2.5. The fracture mechanics parameters $\Delta K$, $K_{max}$, $J_{el}$ and $J$ have no corrosion related dependency, and in particular have no time dependency. Therefore, there is need to develop new parameters that incorporate time dependency in order to capture the frequency effects in CFCG behaviour of materials.

The variation of $\Delta K$ with time in CFCG tests is demonstrated in Fig. 9 while the equivalent graphs showing $J$ plotted against time are shown in Fig. 10. It can be seen in these figures that $\Delta K$ and $J$ increase monotonically as time passes. As seen in Equations (10) and (14)–(16), the fracture mechanics parameters $\Delta K$ and $J$ are proportional to the crack length. This means that during fatigue tests in air and seawater environments the value of fracture mechanics parameter increases with an increase in the crack length. However, it is important to note that the crack growth mechanism in air is solely driven by fatigue while in corrosion-fatigue (i.e. fatigue in seawater environment) this would be due to the combination of corrosion (which is a function of time) and fatigue (which is a function of number of cycles) damage mechanisms. In experiment P10–F0.2, with $P_{max}$ of 10 kN and $f$ of 0.2 Hz, the crack propagation took longer to commence compared with the other CFCG tests performed at 10 kN maximum load. Importantly, it is clear that the slope of the trends become increasingly steep as time passes. Therefore, the rates of change of $\Delta K$ and $J$ are the values that increase essentially monotonically as the experiment progresses. The rate of change of $\Delta K$ in the present study is referred to as $\dot{\Delta K}$ (i.e. $d\Delta K/dt$) whereas the rate

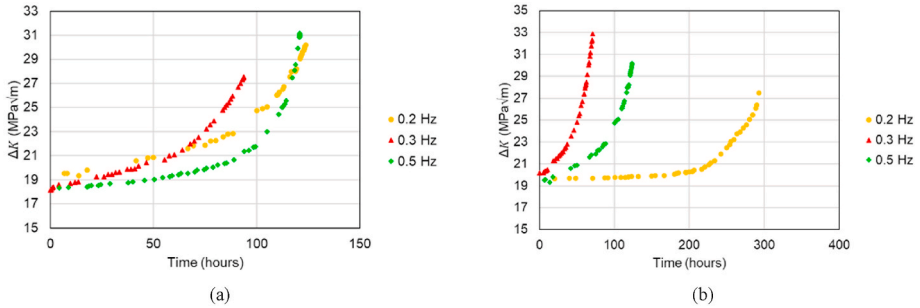


**Fig. 9.** $\Delta K$ vs. time for CFCG tests on S355G10+M steel samples under (a) 9 kN, and (b) 10 kN maximum load.

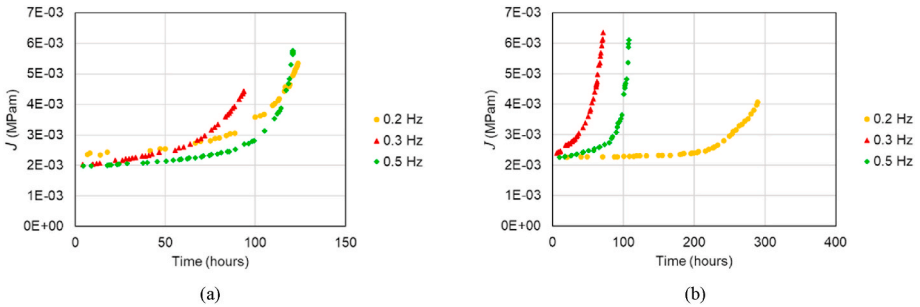


**Fig. 10.** $J$ vs. time for CFCG tests on S355G10+M steel samples under (a) 9 kN, and (b) 10 kN maximum load.

change of $J$ with respect to time is shown as $\dot{J}$ (i.e. $dJ/\,dt$). This provides a link to the time-dependent corrosion aspect of the corrosion-fatigue process, which the previous fracture mechanics parameters (i.e. $\Delta K$ and $J$) lacked, and highlights the need for using a time-dependent fracture mechanics parameter for analysis of the corrosion-fatigue data at different frequencies.

Figs. 11 and 12 show the crack growth rate $da/dN$ against the new time-dependent parameters, $\Delta\dot{K}$ and $\dot{J}$, respectively. The use of these new parameters shows a clearer impact of the frequencies in the range of 0.2–0.5 Hz on the CFCG behaviour of the material. It can be seen in Figs. 11 and 12 that under both $P_{max}$ of 9 kN and 10 kN loading conditions within the inherent experimental scatter the CFCG trend is overall the highest in the lowest frequency experiments conducted at 0.2 Hz, and the lowest in the 0.5 Hz experiments, with 0.3 Hz test results falling in between them. The reducing trend in CFCG behaviour with an increase in the test frequency is more visible in the test data at the maximum load of 10 kN due to less scatter in this data set. The differences in CFCG trends as a result of applying various frequencies appear to diminish as $\Delta\dot{K}$ and $\dot{J}$ increase, with the crack growth rates generally appearing to converge in the latter stages of the experiments. This aligns well with the findings in the literature where the frequency effects have been found to be less significant towards the end of the tests when the crack growth rates were correlated with $\Delta K$ (Fatoba, 2016) (Menan and Henaff, 2009). These results clearly show that the dependency of the CFCG behaviour of the material on the test frequency will be only revealed when the crack growth rates are correlated with a time-dependent fracture mechanics parameter such as $\Delta\dot{K}$ and $\dot{J}$.

The mechanisms causing the increased crack growth rate in the corrosive environment are likely to be a combination of anodic dissolution, hydrogen embrittlement and oxygen depolarisation, as S355G10+M is a medium strength steel (Venzlaff et al., 2013) (Chatterjee and Singh Raman, 2011). Hydrogen embrittlement and oxygen depolarisation, which were discussed in Section 2.2, are both affected by the degree of hydrogen present. Hydrogen is produced by the oxidation of the metal at the crack tip and also by hydrolysis, both of which are dependent on time, and hence on the loading frequency (Li et al., 1984). That's why the time-dependent $\Delta\dot{K}$ and $\dot{J}$ show more clearly the impact of changes in frequency through to crack growth rate in the range 0.2–0.5 Hz than the traditional time-independent fracture mechanics parameters.

### 4.4. Appropriateness of $\Delta\dot{K}$ versus $\dot{J}$

The degree of plasticity can affect the crack growth rate by influ-

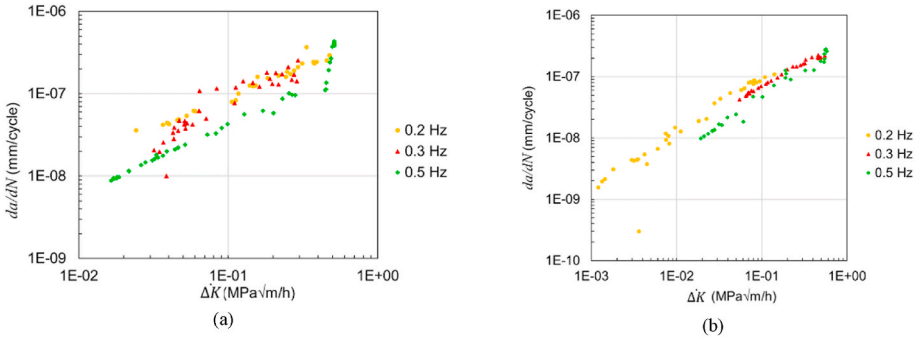


**Fig. 11.** Crack growth rate vs. $\Delta\dot{K}$ for CFCG tests on S355G10+M steel samples under (a) 9 kN, and (b) 10 kN maximum load.

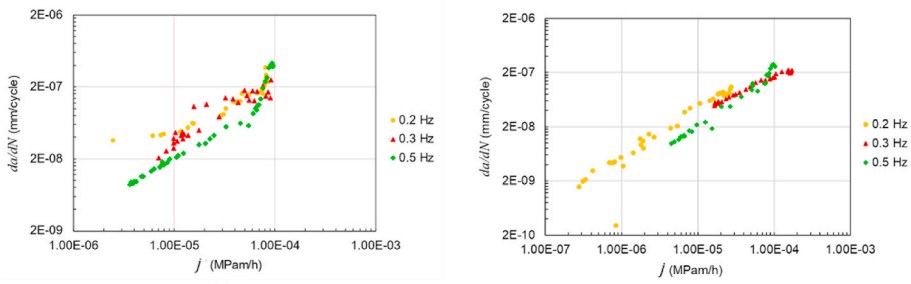


**Fig. 12.** Crack growth rate vs. $\dot{J}$ for CFCG tests on S355G10+M steel samples under (a) 9 kN, and (b) 10 kN maximum load.

**Table 4**
Assessment of degree of plasticity in S355G10+M corrosion-fatigue experiments.

| | $r_p$ (mm) | $\sigma_{ref}/\sigma_{0.2}$ |
|---|---|---|
| P9–F0.2 | 0.45 | 0.31 |
| P9–F0.3 | 0.37 | 0.27 |
| P9–F0.5 | 0.48 | 0.33 |
| P10–F0.2 | 0.37 | 0.25 |
| P10–F0.3 | 0.53 | 0.34 |
| P10–F0.5 | 0.51 | 0.33 |

encing the rate at which hydrogen can penetrate into the metal (Li et al., 1984). The values of the plastic zone size $r_p$ and normlaised reference stress $\sigma_{ref}/\sigma_{0.2}$ at the end of the CFCG tests, calculated under the maximum applied load, are summarised in Table 4. From Table 4 it can be seen that the estimated plastic zone sizes (see Equation (17)) in the CFCG tests were much smaller than the crack lengths. Furthermore, the normalised reference stresses are all substantially less than unity indicating limited plasticity in the cracked specimens (Mehmanparast et al., 2016). Hence, for the S355G10+M steel examined under 9 kN and 10 kN of maximum cyclic load in this study, there is little benefit to consider $\dot{J}$ as a time-dependent corrosion-fatigue parameter which is sensitive to plasticity as opposed to $\Delta\dot{K}$. If greater plasticity is present in other material-environment combinations, then the use of $\dot{J}$ may be preferable to capture the plasticity effect.

## 5. A new time-dependent corrosion-fatigue crack growth model

### 5.1. Model description

A new model based on the time-dependent fracture mechanics parameter $\Delta\dot{K}$ has been inductively developed for predicting the CFCG rates in S355G10+M steel in seawater. The basis of the model is similar to the one described by Anderson where the crack growth rate in a corrosive environment can be predicted from the data in an inert environment (Anderson, 2017). However, the crack growth rate model developed in the present study is described as a function of time-dependent $\Delta\dot{K}$ parameter, rather than $\Delta K$. The structure of the new proposed CFCG model in general form is shown in Equation (19). In this equation, the left-hand side indicates the total CFCG rate $\left(\frac{da}{dN}\right)_{CF}$ evaluated at some value of $\Delta\dot{K}_{CF}$, whereas on the right-hand side $\left(\frac{da}{dN}\right)_{air}$ indicates the crack growth rate of the material in air multiplied by an acceleration parameter $\varphi$, evaluated at the scaled down value of $10^{-\lambda}\,\Delta\dot{K}_{air}$ from the air test, where $\lambda$ is a model parameter. According to the proposed model, the correlation between $\left(\frac{da}{dN}\right)_{CF}$ and $\Delta\dot{K}_{CF}$ for the corrosion-fatigue test can be predicted from the air test by plotting $\varphi\left(\frac{da}{dN}\right)_{air}$ against $10^{-\lambda}\,\Delta\dot{K}_{air}$. This rescaling of the right-hand side of the equation is required as, typically, fatigue experiments conducted in air are undertaken at a frequency much greater (hence higher rate of change) than those of corrosion-fatigue experiments. Generally, the effects of frequency are only seen in corrosion-fatigue tests where the frequency is less than 1 Hz (see Section 2.5) while the frequency has little or no effect in fatigue crack growth tests in air which are typically performed at frequencies of greater than 1 Hz. Therefore, in order to be able to predict corrosion-fatigue behaviour based on results from the air environment, the $\Delta\dot{K}_{air}$ values from air test need to be appropriately rescaled.

$$\left(\frac{da}{dN}\right)_{CF}\left[at\ \Delta\dot{K}_{CF}\right]=\varphi\left(\frac{da}{dN}\right)_{air}\left[at\ 10^{-\lambda}\,\Delta\dot{K}_{air}\right] \tag{19}$$

In Equation (19) $\lambda$ and $\varphi$ parameters can be described as:

$$\lambda=\gamma P_{average}\left(1-\frac{f_{CF}}{f_{air}}\right) \tag{20}$$

$$\varphi=10^{\mu(1-f_{CF})} \tag{21}$$

where $\gamma$ and $\mu$ are material-environment dependent parameters, $P_{average}$ is the average applied load in kN, $f_{CF}$ is the frequency in the corrosion-fatigue experiment in Hz and $f_{air}$ is the frequency in the air experiment in Hz. It is worth noting that $\gamma$ and $\mu$ parameters are both "material" and "environment" dependent, which means these values change if the tested material is changed or for the same material if the testing environment is changed from air to seawater. Even within the seawater environment, if the pH or water temperature is changed the parameters need to be recalibrated.

In order to calibrate the model for a given material and seawater state, γ and μ constants must be identified through an iterative process by minimising the error between the predicted trend and at least one experimental data set. For this purpose, the "least squares method" is employed to find the best fit made to the CFCG data set by effectively shifting the air curve which is used as the baseline for CFCG prediction. After the best fit is made to the CFCG data set, the corresponding values of γ and μ are calculated using the constants obtained from the line of best fit and the definitions provided in Equations (19)–(21). Once the model is calibrated for a given material and environment using a single CFCG data set, it can be used to predict the CFCG trend at different frequencies and load levels.

Equation (20) remains valid as long as the corrosion-fatigue frequency is equal to or less than the one applied in the air test ($f_{CF} \leq f_{air}$ hence $\lambda \geq 0$). The greater $f_{air}$ is than $f_{CF}$, the smaller the ratio $f_{CF}/f_{air}$ becomes, and so the bigger the parameter $\lambda$, and hence the more $\Delta\dot{K}_{air}$ needs to be scaled down to account for the greater difference in frequencies for $\Delta\dot{K}_{CF}$. The value of $f_{CF}$ is assumed to be always less than 1 Hz as suggested by the existing corrosion-fatigue data in the literature, hence $(1 - f_{CF})$ in Equation (21) always takes a value between 0 and 1. The lower the corrosion-fatigue frequency, the greater the value of $\varphi$ will be and hence a greater CFCG rate will be predicted using the proposed model in Equation (19).

The maximum load was found to affect the degree of rescaling required. This may be due to a non-linear relationship between the maximum load and the rate of change of $\Delta K$. The average load, however, is included here in the model rather than the maximal load. This is because the average load also depends on the $R$ ratio and it has been shown in the literature that the $R$ ratio affects the crack growth rate by the trapping of hydrogen at grain boundaries (Li et al., 1984). Therefore, it is considered appropriate to include the average load which incorporates an effect from the $R$ ratio in the proposed model.

### 5.2. Comparison of the modelled and measured crack growth rates for S355G10+M steel

The CFCG results obtained in the present study on S355G10+M steel were analysed and modelled using the proposed approach detailed above. The parameters $\gamma$ and $\mu$ for this material and environment (with the given pH and water temperature) were found via an iterative process by employing the least squares method conducted in MATLAB. For this purpose, the fatigue data set in air and the first CFCG data set for S355G10+M steel with the frequency of 0.2 Hz and the maximum load level of 9 kN were utilised to identify and calibrate $\gamma$ and $\mu$ parameters (see Fig. 13(a)). Following the calibration process, the material-environment dependent parameters $\gamma$ and $\mu$ were found to be 0.08 and 1.15, respectively, and subsequently the CFCG trends were modelled and predicted for the rest of the frequencies and load levels. The comparison of the modelled CFCG trends with the experimental results are shown in Figs. 13, Figs. 14 and 15 for the test frequencies of 0.2, 0.3 and 0.5 Hz, respectively. In general, very good agreements have been found between the experimental data and the predicted trends for different frequencies. One drawback of the model is that any scatter, anomalies or discontinuities in the air data are carried over into the CFCG predictions, as is seen in the dip in the trends for the 10 kN maximum load case. Having said that, the overall trends in the model predictions are clearly well aligned with the measured data in all instances. Moreover, the results show that the CFCG behaviour of the material can be accurately predicted using short-term test data in air, which can be completed in much shorter time scales at higher frequencies, without the need to perform long-term corrosion-fatigue tests at low frequencies.

In the case of CFCG test at $P_{max} = 10$ kN and $f = 0.2$ Hz, there is however a slight disagreement on the range of $\Delta\dot{K}$, with the measured values beginning earlier than the modelled and also ending earlier. However, as was seen in Fig. 9, this particular CFCG test was unusual in its slow commencement of crack propagation, which has led to unusually low values of $\Delta\dot{K}$ not seen in any of the other tests. Therefore, the less perfect prediction of $\Delta\dot{K}$ values by the model in this instance may in fact be due to an anomaly in the measured data. Finally, yet importantly, it can be seen in Figs. 13, Figs. 14 and 15 that the identified $\gamma$ and $\mu$ parameters for S355G10+M steel have resulted in very good predictions of the CFCG trends for two different loading conditions confirming that these two parameters are material-environment dependent and do not depend on the loading conditions.

### 5.3. Comparison of the modelled and measured crack growth rates for S355J2+N steel

The proposed model in this study has also been applied to another subgrade of S355 steel found in the literature. S355J2+N steel is generally used for the primary structures in offshore wind foundations (Igwemezie and Mehmanparast, 2020). The 'J2' indicates a notch impact test conducted at −20 °C and the +N indicates normalised weldable fine grain structural steel (Igwemezie and Mehmanparast, 2020). In a previous work by Adedipe et al. corrosion-fatigue experiments were conducted on S355J2+N steel C(T) specimens in seawater at various frequencies (Adedipe et al., 2015). These tests were conducted under 10 kN maximum load and $R$ ratio of 0.1 at frequencies of 0.35 and 0.4 Hz. The experimental data presented in their study has been re-analysed here to plot the crack growth rate against $\Delta\dot{K}$ from these tests. The material-environment dependent parameters $\gamma$ and $\mu$ for S355J2+N steel were found to be 0.15 and 0.20, respectively, via an iterative process conducted in MATLAB, using the fatigue data set in air and the first CFCG data set with the frequency of 0.35 Hz and maximum load of 10 kN (see Fig. 16(a)). Subsequently, the CFCG trend for the other frequency of 0.4 Hz (see Fig. 16(b)) was modelled and predicted. Fig. 16 shows that very good agreement has been found between the modelled and the measured CFCG results at both frequencies of 0.35 and 0.4 Hz. This is aided by the smoothness in the trends of the data obtained from the experiments in air, which are translated through to a smooth prediction for the corrosion-fatigue behaviour.

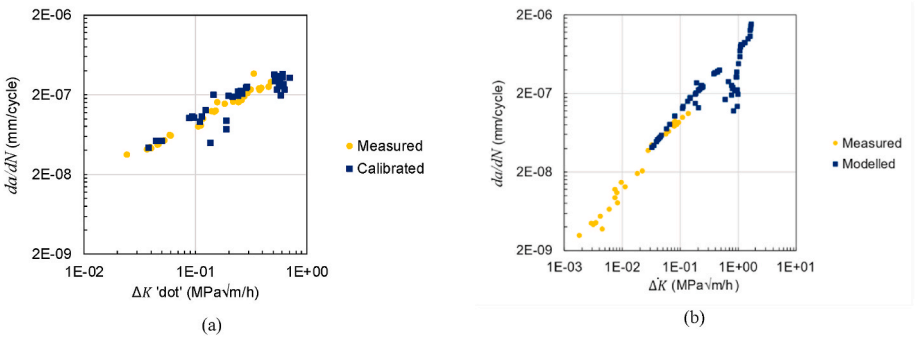


**Fig. 13.** Analysis of the experimentally measured CFCG data for S355G10+M steel at 0.2 Hz frequency and comparison with (a) calibrated curve fit for 9 kN maximum load data set, (b) modelled CFCG rates against $\Delta\dot{K}$ for 10 kN maximum load data.

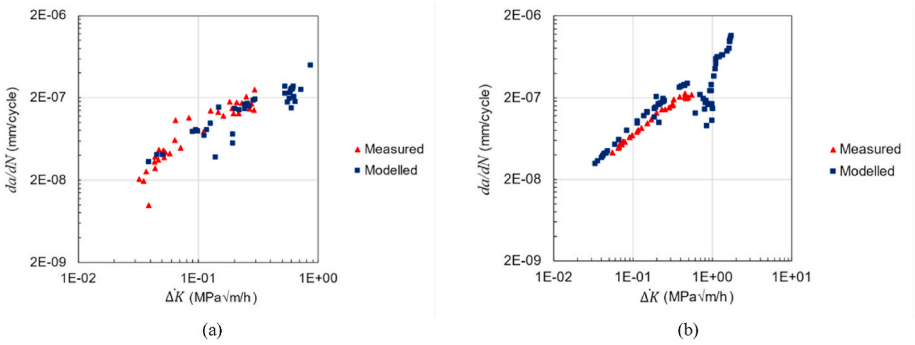


**Fig. 14.** Analysis of the experimentally measured and modelled CFCG rates against $\Delta\dot{K}$ for S355G10+M steel at 0.3 Hz frequency under (a) 9 kN and (b) 10 kN maximum load.

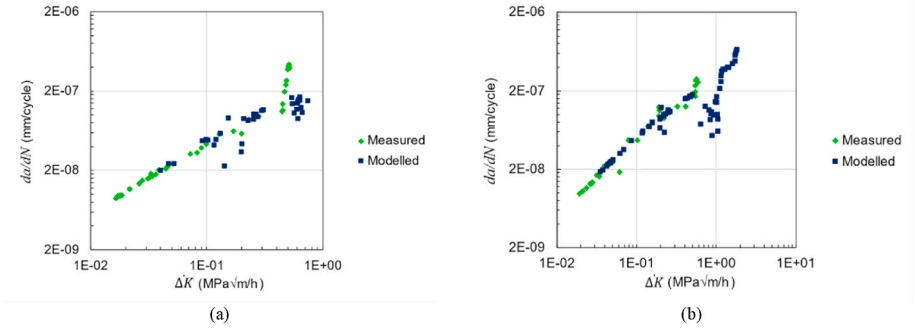


**Fig. 15.** Analysis of the experimentally measured and modelled CFCG rates against $\Delta\dot{K}$ for S355G10+M steel at 0.5 Hz frequency under (a) 9 kN and (b) 10 kN maximum load.

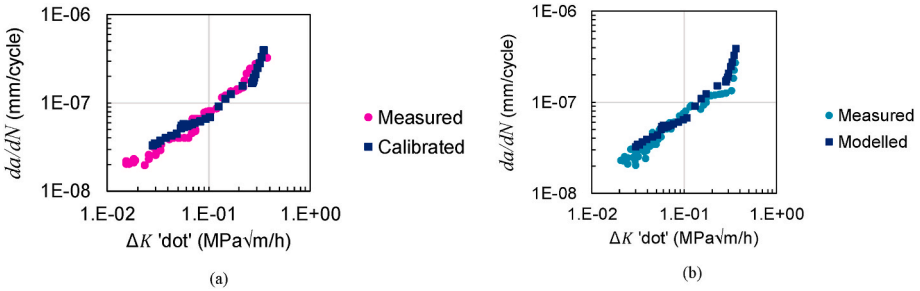


**Fig. 16.** Analysis of the experimentally measured CFCG data for S355J2+N steel and comparison with (a) calibrated curve fit for 0.35 Hz frequency data set, (b) modelled CFCG rates against $\Delta\dot{K}$ for 0.4 Hz frequency data set.

### *5.4. Overall discussion and future work*

The results from this study show that the proposed model can be used to accurately predict the CFCG behaviour of various steel structures at different frequencies using the short-term air data and by means of a time-dependent fracture mechanics parameter. The CFCG data sets which were considered and analysed in this study were obtained from the tests with loading conditions that had resulted in limited plasticity in the specimens, hence $\Delta\dot{K}$ was successfully implemented in the model to predict the CFCG rates at various frequencies. In the case that there is significant level of plasticity in the cracked specimens, the suitability of the time-dependent $\dot{J}$ parameter, instead of $\Delta\dot{K}$, will be examined in future work using a similar approach described in Section 5.1.

It is difficult to apply the model directly to other existing data in the literature as generally insufficient information is included in published work to calculate $\Delta\dot{K}$, as the cycle number and frequency (or time) of each $\Delta K$ value is required. However, a collaborative piece of work could allow for the application of the model to a wide range of existing material-environment experiments that have already been conducted, via the sharing of the relevant details from researchers, without the need for an extensive set of new experiments. This would allow for the creation of a bank of data for the model parameters $\gamma$ and $\mu$, which would allow for easy application of the model to a wide range of steels. This would also allow for a deeper dive into the use of the new time-dependent parameters more generally.

Further experiments in future work by varying the $R$ ratio could validate the influence that this factor may have on the model that may not already captured by $P_{average}$ parameter. The cyclic waveform shapes have also been shown to affect CFCG rates (Igwemezie and Mehmanparast, 2020), so the model could also be extended in future work for use beyond the sinusoidal waveform. This may be feasible through examination of existing evidence in the literature, but additional focused experiments may be required. The materials examined in this study were made of base metal, so another future work will be to investigate the characterisation of CFCG behaviour in welded joints with more complex material microstructures using the approach proposed in this study.

## 6. Conclusions

Corrosion-fatigue is known to be the dominant failure mechanism in offshore structures, such as offshore wind turbine foundations, which need to be fully understood and characterised for reliable life predictions in engineering structures. In this study, a range of existing models for describing corrosion-fatigue behaviour of various engineering materials were thoroughly reviewed. It was found out that the existing models, the majority of which are dependent on $\Delta K$ fracture mechanics parameter, are insensitive to the test frequency in corrosion-fatigue tests. To fill in this gap in the knowledge, new time-dependent fracture mechanics parameters, $\Delta\dot{K}$ and $\dot{J}$, were developed and employed in the analysis of the CFCG data. It has been shown that depending on the level of plasticity in the test specimens, one of these parameters ($\Delta\dot{K}$ for limited plasticity and $\dot{J}$ for widespread plasticity) can be employed to describe the CFCG rate in steel structures at various frequencies. Subsequently, a new model was developed for predicting the CFCG rate from the crack growth data in air using the time-dependent $\Delta\dot{K}$ parameter. The model predictions have been validated through comparison with the experimental data on S355G10+M obtained from this study and S355J2+N data from the literature. Good agreements were found between the modelled and measured CFCG rates for both materials at different frequencies. The proposed model suggests that in the absence of significant plasticity the CFCG trends at different frequencies can be predicted using the short-term air data and the time-dependent fracture mechanics parameter $\Delta\dot{K}$. The prediction of CFCG rates in the presence of significant plasticity will be conducted in future work to further examine the suitability of $\dot{J}$ parameter for CFCG prediction.

## Credit author statement

**Helen Ryan:** Methodology, Validation, Formal analysis, Writing - Original Draft. **Ali Mehmanparast:** Conceptualization, Resources, Writing - Review & Editing, Supervision

## Declaration of competing interest

The authors declare that they have no known competing financial interests or personal relationships that could have appeared to influence the work reported in this paper.

## Data availability

Data will be made available on request.

## Acknowledgments

This work was supported by grant EP/L016303/1 for Cranfield, Oxford and Strathclyde Universities' Centre for Doctoral Training in Renewable Energy Marine Structures – REMS CDT (http://www.rems-cdt.ac.uk/) from the UK Engineering and Physical Sciences Research Council (EPSRC).

## References

4coffshore, 2021. Global offshore wind farm database. Available at: https://www.4coffshore.com/. (Accessed 10 July 2021).
Adedipe, O., Brennan, F., Kolios, A., 2015. Corrosion fatigue load frequency sensitivity analysis. Mar. Struct. 42 https://doi.org/10.1016/j.marstruc.2015.03.005.
Anderson, T.L., 2017. Fracture Mechanics : Fundamentals and Applications, fourth ed. Taylor & Francis Group.
ASTM International, 2015. ASTM E647-15. In: Standard Test Method for Measurement of Fatigue Crack Growth Rates. West Conshohocken.
ASTM International, 2021. ASTM D1141 - 98: Standard Practice for Preparation of Substitute Ocean Water.
Austen, I.M., Mcintyre, P., 1979. Corrosion fatigue of high-strength steel in low-pressure hydrogen gas. Met. Sci. 13 (7) https://doi.org/10.1179/msc.1979.13.7.420.
Austen, I.M., Walker, E.F., 1977. Quantitative understanding of the effects of mechanical and environmental variables on corrosion fatigue crack growth behaviour. In: The Influence of Environment on Fatigue. Institution of Mechanical Engineers, London, pp. 1–10.
Balbín, J.A., Chaves, V., Larrosa, N.O., 2021. Pit to crack transition and corrosion fatigue lifetime reduction estimations by means of a short crack microstructural model. Corrosion Sci. 180, 109171 https://doi.org/10.1016/j.corsci.2020.109171.
BloombergNEF, 2020. Scale-up of solar and wind puts existing coal, gas at risk. Available at: https://about.bnef.com/blog/scale-up-of-solar-and-wind-puts-existing-coal-gas-at-risk/. (Accessed 1 August 2021).
British Standard, 2008. BS EN ISO 11782-2: Corrosion of Metals and Alloys — Corrosion Fatigue Testing —Part 2: Crack Propagation Testing Using Precracked Specimens. BSI.
British Standard, 2019. BS 7910:2019 Guide to Methods for Assessing the Acceptability of Flaws in Metallic Structures. BSI.
Chatterjee, U.K., Singh Raman, R.K., 2011. Stress corrosion cracking (SCC) in low and medium strength carbon steels. In: Stress Corrosion Cracking. Elsevier. https://doi.org/10.1533/9780857093769.3.169.
Etris, S., Lieb, K., Sisca, V., Moore, I., Batik, A., Miller, G., Hudak, S., Wei, R., 1973. The influence of loading variables on environment-enhanced fatigue crack growth in high strength steels. J. Test. Eval. 1 (6) https://doi.org/10.1520/JTE10062J.
Fatoba, O., 2016. Experimental and Modelling Studies of Corrosion Fatigue Damage in a Linepipe Steel.
Fatoba, O.O., Leiva-Garcia, R., Lishchuk, S.V., Larrosa, N.O., Akid, R., 2018. Simulation of stress-assisted localised corrosion using a cellular automaton finite element approach. Corrosion Sci. 137 https://doi.org/10.1016/j.corsci.2018.03.029.
Fernández-Sousa, R., Betegón, C., Martínez-Paneda, E., 2022. Cohesive zone modelling of hydrogen assisted fatigue crack growth: the role of trapping. Int. J. Fatig. 162, 106935 https://doi.org/10.1016/j.ijfatigue.2022.106935.
Hu, H., 1997. Fatigue and Corrosion Fatigue Crack Growth Resistance of RQT501.
Igwemezie, V., Mehmanparast, A., 2020. Waveform and frequency effects on corrosion-fatigue crack growth behaviour in modern marine steels. Int. J. Fatig. 134 https://doi.org/10.1016/j.ijfatigue.2020.105484.
Igwemezie, V., Mehmanparast, A., Kolios, A., 2019. Current trend in offshore wind energy sector and material requirements for fatigue resistance improvement in large wind turbine support structures – a review. Renew. Sustain. Energy Rev. 101 https://doi.org/10.1016/j.rser.2018.11.002.
Jacob, A., Oliveira, J., Mehmanparast, A., Hosseinzadeh, F., Kelleher, J., Berto, F., 2018. Residual stress measurements in offshore wind monopile weldments using neutron diffraction technique and contour method. Theor. Appl. Fract. Mech. 96, 418–427. https://doi.org/10.1016/j.tafmec.2018.06.001.
Jaske, C., Payer, J., Balint, V., 1981. Corrosion Fatigue of Metals in Marine Environments. Springer Verlag.
Kalnaus, S., Zhang, J., Jiang, Y., 2011. Stress-corrosion cracking of AISI 4340 steel in aqueous environments. Metall. Mater. Trans. 42 (2) https://doi.org/10.1007/s11661-010-0335-y.
Kim, S.S., Choe, S.J., Shin, K.S., 1998. Quantitative models on corrosion fatigue crack growth rates in metals: Part I. Overview of quantitative crack growth models. Met. Mater. 4 (1) https://doi.org/10.1007/BF03026059.
Kondo, Y., 1989. Prediction of fatigue crack initiation life based on pit growth. Corrosion 45 (1). https://doi.org/10.5006/1.3577891.
Larrosa, N.O., Chapetti, M.D., Ainsworth, R.A., 2016. Fatigue life estimation of pitted specimens by means of an integrated fracture mechanics approach. In: Pressure Vessels and Piping Conference, vol. 50398. American Society of Mechanical Engineers, V003T03A057.
Larrosa, N.O., Akid, R., Ainsworth, R.A., 2018. Corrosion-fatigue: a review of damage tolerance models. Int. Mater. Rev. 63 (5) https://doi.org/10.1080/09506608.2017.1375644.
Li, S.-X., Akid, R., 2013. Corrosion fatigue life prediction of a steel shaft material in seawater. Eng. Fail. Anal. 34 https://doi.org/10.1016/j.engfailanal.2013.08.004.
Li, M.-Q., Shi, Y., Tong, Z., 1984. An investigation of corrosion fatigue of some low alloy steelsin aqueous nacl solution. J. Chin. Soc. Corrosion Protect 4 (1), 61–69.
Li, M.-Q., Wei, Z.-W., Zhang, F.-S., Tang, J.-Q., 1993. The corrosion fatigue of medium strength structural steels. Corrosion Sci. 34 (9) https://doi.org/10.1016/0010-938X(93)90236-A.
McEvily, A., Wei, R., 1972. Fracture mechanics and corrosion fatigue. In: Corrosion Fatigue: Chemistry, Mechanics and Microstructure NACE-2, pp. 381–395.
Mehmanparast, A., 2012. The Influence of Inelastic Damage on Creep, Fatigue and Fracture Toughness.
Mehmanparast, A., Davies, C.M., Dean, D.W., Nikbin, K., 2016. Effects of plastic pre-straining level on the creep deformation, crack initiation and growth behaviour of 316H stainless steel. Int. J. Pres. Ves. Pip. 141 https://doi.org/10.1016/j.ijpvp.2016.03.013.
Mehmanparast, A., Albani, P., Igwemezie, V., 2018. Crack growth monitoring in corrosion-fatigue tests using back face strain measurement technique. Procedia Struct. Integr. 13 https://doi.org/10.1016/j.prostr.2018.12.044.
Menan, F., Henaff, G., 2009. Influence of frequency and exposure to a saline solution on the corrosion fatigue crack growth behavior of the aluminum alloy 2024. Int. J. Fatig. 31 (11–12) https://doi.org/10.1016/j.ijfatigue.2009.02.033.
Seifert, H.-P., Hickling, J., Lister, D., 2012. Corrosion and environmentally-assisted cracking of carbon and low-alloy steels. In: Comprehensive Nuclear Materials. Elsevier. https://doi.org/10.1016/B978-0-08-056033-5.00081-1.
Sriraman, M.R., Pidaparti, R.M., 2009. Life prediction of aircraft aluminum subjected to pitting corrosion under fatigue conditions. J. Aircraft 46 (4). https://doi.org/10.2514/1.40481.

The Intergovernmental Panel on Climate Change, 2021. Climate Change 2021: the Physical Science Basis.
Venzlaff, H., Enning, D., Srinivasan, J., Mayrhofer, K.J.J., Hassel, A.W., Widdel, F., Stratmann, M., 2013. Accelerated cathodic reaction in microbial corrosion of iron due to direct electron uptake by sulfate-reducing bacteria. Corrosion Sci. 66 https://doi.org/10.1016/j.corsci.2012.09.006.
Vosikovsky, O., 1975. Fatigue-crack growth in an X-65 line-pipe steel at low cyclic frequencies in aqueous environments. J. Eng. Mater. Technol. 97 (4) https://doi.org/10.1115/1.3443302.
Wang, Q.Y., Pidaparti, R.M., Palakal, M.J., 2001. Comparative study of corrosion-fatigue in aircraft materials. AIAA J. 39 (2) https://doi.org/10.2514/2.1308.
Wei, R., 1978. On understanding environment-enhanced fatigue crack growth — a fundamental approach. In: Fatigue Mechanisms. 100 Barr Harbor Drive, PO Box C700. ASTM International, West Conshohocken, PA 19428-2959. https://doi.org/10.1520/STP35916S.
Wei, R.P., Gao, M., 1983. Reconsideration of the superposition model for environmentally assisted fatigue crack growth. Scripta Metall. 17 (7) https://doi.org/10.1016/0036-9748(83)90270-3.
Wei, R.P., Landes, J.D., 1969. Correlation between sustained-load and fatigue crack growth in high-strength steels. Mater. Res. Stand. 9 (7), 25–46.
Wei, R.P., Simmons, G.W., 1981. Recent progress in understanding environment assisted fatigue crack growth. Int. J. Fract. 17 (2) https://doi.org/10.1007/BF00053522.
Weng, L., Zhang, J., Kalnaus, S., Feng, M., Jiang, Y., 2013. Corrosion fatigue crack growth of AISI 4340 steel. Int. J. Fatig. 48 https://doi.org/10.1016/j.ijfatigue.2012.10.015.
Xin, H., Veljkovic, M., 2020. Residual stress effects on fatigue crack growth rate of mild steel S355 exposed to air and seawater environments. Mater. Des. 193 https://doi.org/10.1016/j.matdes.2020.108732.
Yu, Y., Sun, W., Tong, D., 2020. Effect of loading frequency on corrosion fatigue crack growth rate of 7N01 aluminum alloy. IOP Conf. Ser. Mater. Sci. Eng. 768 https://doi.org/10.1088/1757-899X/768/2/022060.